

Article

Efficient Bias-Free Degradation of Sulfamethazine by TiO₂ Nanoneedle Arrays Photoanode and Co₃O₄ Photocathode System under LED-Light Irradiation

Zhongzheng Hu ^{1,2,†}, Ruiheng Liang ^{1,2,†}, Xiangru Song ^{1,2}, Huizhong Wu ^{1,2}, Jiangli Sun ^{1,2}, Jingyang Liu ^{1,2}, Minghua Zhou ^{1,2,*} and Omotayo A. Arotiba ^{3,4} 

¹ Tianjin Key Laboratory of Environmental Technology for Complex Trans-Media Pollution, College of Environmental Science and Engineering, Nankai University, Tianjin 300350, China

² Tianjin Advanced Water Treatment Technology International Joint Research Center, College of Environmental Science and Engineering, Nankai University, Tianjin 300350, China

³ Department of Chemical Sciences, University of Johannesburg, Doornfontein, Johannesburg 2028, South Africa

⁴ Centre for Nanomaterials Science Research, University of Johannesburg, Johannesburg 2028, South Africa

* Correspondence: zhoumh@nankai.edu.cn

† These authors contributed equally to this work.

Abstract: Solving high electrical-energy input for pollutants degradation is one of the core requirements for the practical application of photoelectrocatalytic (PEC) technology. Herein, we developed a self-driven dual-photoelectrode PEC system (TiO₂ NNs-Co₃O₄) composed of a TiO₂ nanoneedle arrays (TiO₂ NNs) photoanode and Co₃O₄ photocathode for the first time. Under light-emitting-diode (LED) illumination, the bias-free TiO₂ NNs-Co₃O₄ PEC system exhibited excellent PEC performance, with an internal bias as high as 0.19 V, achieving near complete degradation (99.62%) of sulfamethazine (SMT) with a pseudo-first-order rate constant of 0.042 min⁻¹. The influences of solution pH, typical inorganic anions, natural organic matter, and initial SMT concentration on the PEC performance were investigated. Moreover, the main reactive oxygen species (h⁺, •OH, •O₂⁻) in the dual-photoelectrode PEC system for SMT decomposition were elaborated. The practical application feasibility for efficient water purification of this unbiased PEC system was evaluated. It was proved that the TiO₂ NNs photoanode provided a negative bias while the Co₃O₄ photocathode provided a positive bias for the photoanode, which made this system operate without external bias. This work elucidated the cooperative mechanism of photoelectrodes, providing guidance to develop a sustainable, efficient, and energy-saving PEC system for wastewater treatment.

Keywords: photoelectrocatalysis; dual-photoelectrode; light-emitting diodes; sulfamethazine; mechanism



Citation: Hu, Z.; Liang, R.; Song, X.; Wu, H.; Sun, J.; Liu, J.; Zhou, M.; Arotiba, O.A. Efficient Bias-Free Degradation of Sulfamethazine by TiO₂ Nanoneedle Arrays Photoanode and Co₃O₄ Photocathode System under LED-Light Irradiation. *Catalysts* **2023**, *13*, 327. <https://doi.org/10.3390/catal13020327>

Academic Editors: Xiangjiu Guan and Shichao Zong

Received: 31 December 2022

Revised: 29 January 2023

Accepted: 30 January 2023

Published: 1 February 2023



Copyright: © 2023 by the authors. Licensee MDPI, Basel, Switzerland. This article is an open access article distributed under the terms and conditions of the Creative Commons Attribution (CC BY) license (<https://creativecommons.org/licenses/by/4.0/>).

1. Introduction

As a typical sulfonamide antibiotic, sulfamethazine (SMT) has been used frequently in aquaculture and animal husbandry [1]. SMT has been detected in various aquatic environments, such as underground water, seawater, and river water, and its concentration in the aquatic environment ranges from ng L⁻¹ to µg L⁻¹ [2]. The residue of SMT in aquatic environments may increase bacterial resistance and can bring potential risk to the ecological system and human health through bioaccumulation in the food chain [3,4]. However, traditional bioprocesses cannot efficiently remove SMT, due to its biodegradation resistance [5,6]. Therefore, there is an urgent need to develop a cost-effective and environmentally friendly method to remove SMT.

Advanced oxidation processes (AOPs) have been widely used for degrading refractory organic pollutants [7]. Among various AOPs, photoelectrocatalysis (PEC) has attracted extensive attention for its efficient ability to remove organic pollutants without producing

any harmful by-products [8,9]. Compared with photocatalytic technologies, PEC can accelerate the photogenerated carrier separation and transfer by applying the bias, which achieves a better photoelectric performance. Unfortunately, traditional PEC systems require an external bias to drive the PEC process, which means additional cost for the external power. To lower energy demand, a self-driven dual-photoelectrode PEC system connected with a photoanode and photocathode has been developed [10,11]. Specifically, the dual-photoelectrode PEC system includes two light absorbers: photoanode and photocathode, where the Fermi level difference between photoelectrodes will form an interior photovoltage [12]. The interior photovoltage can offset the electric energy input of the PEC system required to drive the reaction of pollutants removal [13].

In addition, the development of PEC technology has greatly promoted the application of energy-saving and green light-emitting diodes (LEDs). Compared with traditional light sources (such as xenon lamp, halogen lamp), the LED lamp has the advantages of low cost, long service life, low heat production, small size, and high energy conversion, and can be used as the excitation light source of semiconductor materials [14,15]. Therefore, the LED lamp with low energy consumption has great potential in PEC technology to solve environmental problems.

Herein, the novel dual-photoelectrode PEC system was developed, which could efficiently degrade SMT without external voltage. In this self-driven PEC system (named TiO₂ NNs-Co₃O₄), two 30 W LED lamps were served as the light source, TiO₂ nanoneedle arrays (TiO₂ NNs, n-type semiconductor) were used as the photoanode, and Co₃O₄ (p-type semiconductor) was selected as the photocathode. Afterward, the catalytic performance and operating mechanism of the unbiased TiO₂ NNs-Co₃O₄ PEC system under LED light irradiation was systematically studied. The effects of solution pH, typical anions, natural organic matter, initial SMT concentration, recycling, and actual water matrices on the catalytic performance of the TiO₂ NNs-Co₃O₄ system were also deeply investigated to evaluate the practical feasibility.

2. Results and Discussion

2.1. Characterization of Photoelectrodes

The FESEM images of the Ti mesh in Figure 1a manifested that the surface of the Ti mesh was rough and there were a large number of fine grids, which might be conducive to the growth of catalysts [16]. After hydrothermal and annealing treatment, TiO₂ was densely and radially grown around Ti wires to form nanoneedle arrays, whose length was about 1.0 μm. The results were consistent with the literature (Figure 1b–d) [17]. In addition, the morphology of the Co₃O₄ photocathode was shown in Figure 1e–h. It could be seen from Figure 1e,f that Co₃O₄ nanoneedle arrays were evenly distributed onto the Ti mesh support, and the Co₃O₄ nanoneedle had a length of ~4.6 μm, which was composed of densely packed, small nanoparticles (Figure 1g,h) [18].

XRD patterns were recorded in Figure 2a. Notably, the dominant diffraction peaks of Co₃O₄ at 19.0°, 31.2°, 36.8°, 38.5°, 44.8°, 59.3°, and 65.2° might be assigned to the (111), (220), (311), (222), (400), (511), and (440) planes of cubic structure (JCPDS No. 73-1701). Similarly, through diffraction peaks of TiO₂ NNs, it was postulated that the XRD pattern of the TiO₂ NNs electrode was associated with tetragonal rutile TiO₂ (JCPDS No. 21-1276), in agreement with a previous report [19]. The additional peaks on the XRD patterns of the two electrodes should be due to the Ti mesh, and there was no impurity diffraction peak [20]. The results confirmed that TiO₂ NNs and Co₃O₄ photocatalysts had been successfully grown on the Ti mesh.

In addition, XPS was employed to investigate the composition and chemical states of the element. It could be seen from Figure 2b that the Ti and O were included in the XPS full-survey spectra of the TiO₂ NNs photoanode, and the Co and O were included in the XPS full-survey spectra of the Co₃O₄ photocathode. The peaks were located at 458.5 eV and 464.2 eV in the high-resolution Ti 2p XPS spectrum corresponding to the Ti⁴⁺ 2p_{3/2} and Ti⁴⁺ 2p_{1/2} in the TiO₂ lattice, which was consistent with a previous report (Figure 2c) [21].

For the Co_3O_4 photocathode, the prominent peaks of Co 2p spectra were centered at 779.9 eV (Co^{3+}), 781.2 eV (Co^{2+}), 794.8 eV (Co^{3+}), and 796.1 eV (Co^{2+}), indicating that Co^{2+} and Co^{3+} coexisted (Figure 2d) [22]. Based on the above results, it could be perceived that the TiO_2 NNs photoanode and Co_3O_4 photocathode were successfully prepared.

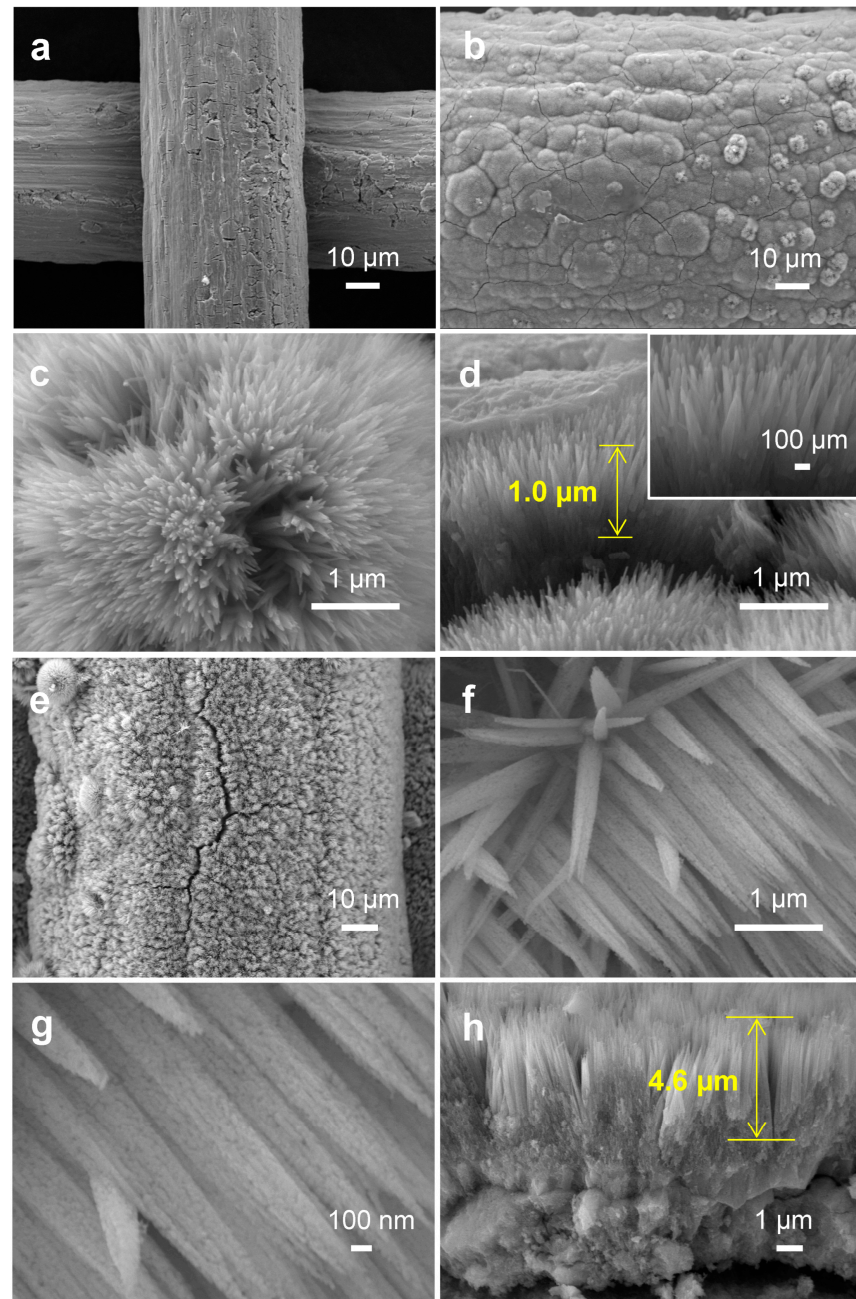


Figure 1. (a) FESEM image of Ti mesh. (b,c) FESEM image and (d) cross-sectional FESEM image of TiO_2 NNs. (e–g) FESEM image and (h) cross-sectional FESEM image of Co_3O_4 .

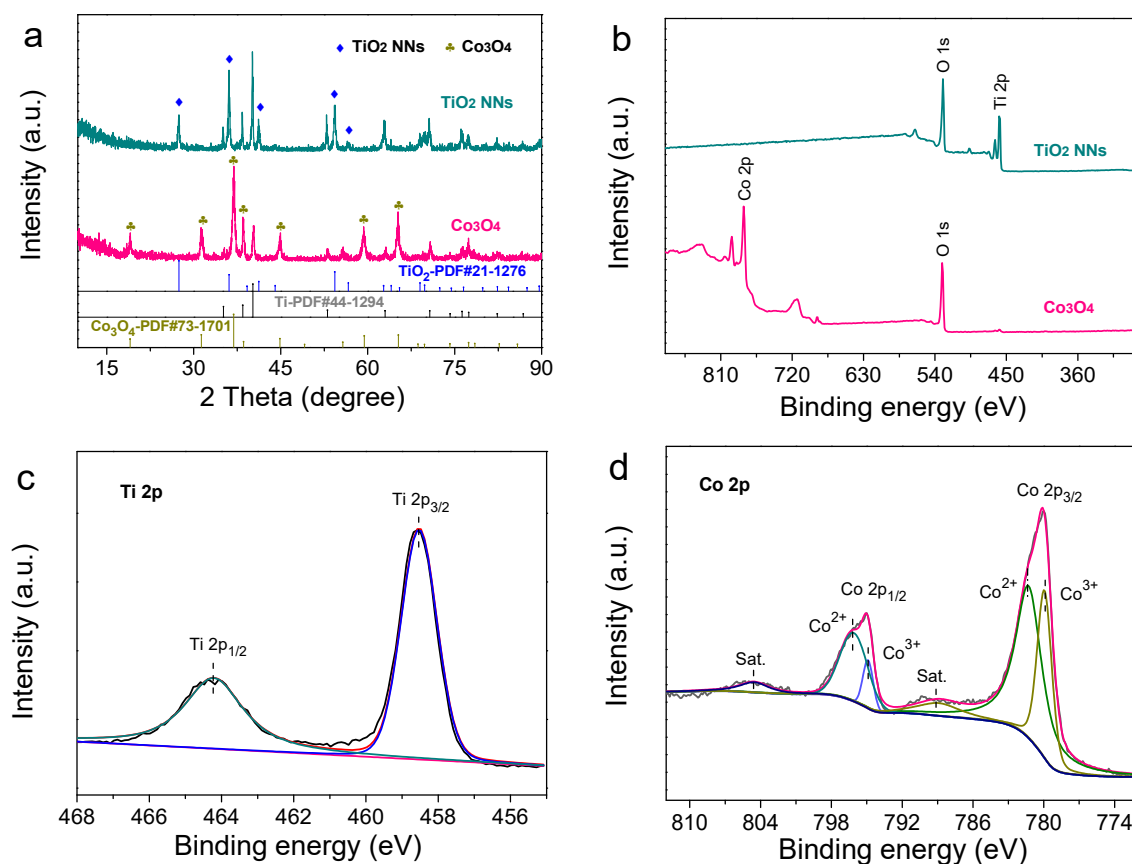


Figure 2. (a) XRD patterns of TiO₂ NNs, Co₃O₄. (b) The full XPS spectra recorded from the surface for TiO₂ NNs and Co₃O₄. High-resolution XPS spectra of Ti 2p (c) and Co 2p (d).

2.2. Photoelectric Properties

The light absorption ability and energy band position were studied. As demonstrated in Figure 3a,c, the absorption edge and valence band (E_{VB}) of the TiO₂ NNs photoanode were around 414 nm and 2.75 eV, respectively. The bandgap (E_g) and conduction band (E_{CB}) were calculated by using Equations (1) and (2) [23].

$$\alpha h\nu = A(h\nu - E_g)^{0.5 \text{ or } 2} \quad (1)$$

$$E_{CB} = E_{VB} - E_g \quad (2)$$

where α , h , and ν are the coefficient, the frequency of light, and Planck's constant, respectively; A is the proportionality constant; 0.5 indicates direct-bandgap semiconductors and 2 indicates indirect semiconductors. Thus, the E_g and E_{CB} of the TiO₂ NNs photoanode were 3.01 eV and -0.26 eV, respectively, consistent with the literature [21]. Similar analysis was also carried out for the Co₃O₄ photocathode and the results were shown in Figure 3b,d. The Co₃O₄ photocathode could absorb ultraviolet and light, whose E_g , E_{VB} , and E_{CB} were 2.30 eV, 0.80 eV, and -1.50 eV, respectively. As expected, the Fermi level of the n-type TiO₂ NNs semiconductor was close to conduction band (-0.26 eV), and the Fermi level of the p-type Co₃O₄ semiconductor was close to the valence band (0.80 eV) [24]. The TiO₂ NNs photoanode and Co₃O₄ photocathode were combined to construct a novel dual-photoelectrode PEC system [12]. As is known, the internal bias was generated by the Fermi level difference of the electrodes, which made it possible to establish a self-driven TiO₂ NNs-Co₃O₄ PEC system [25].

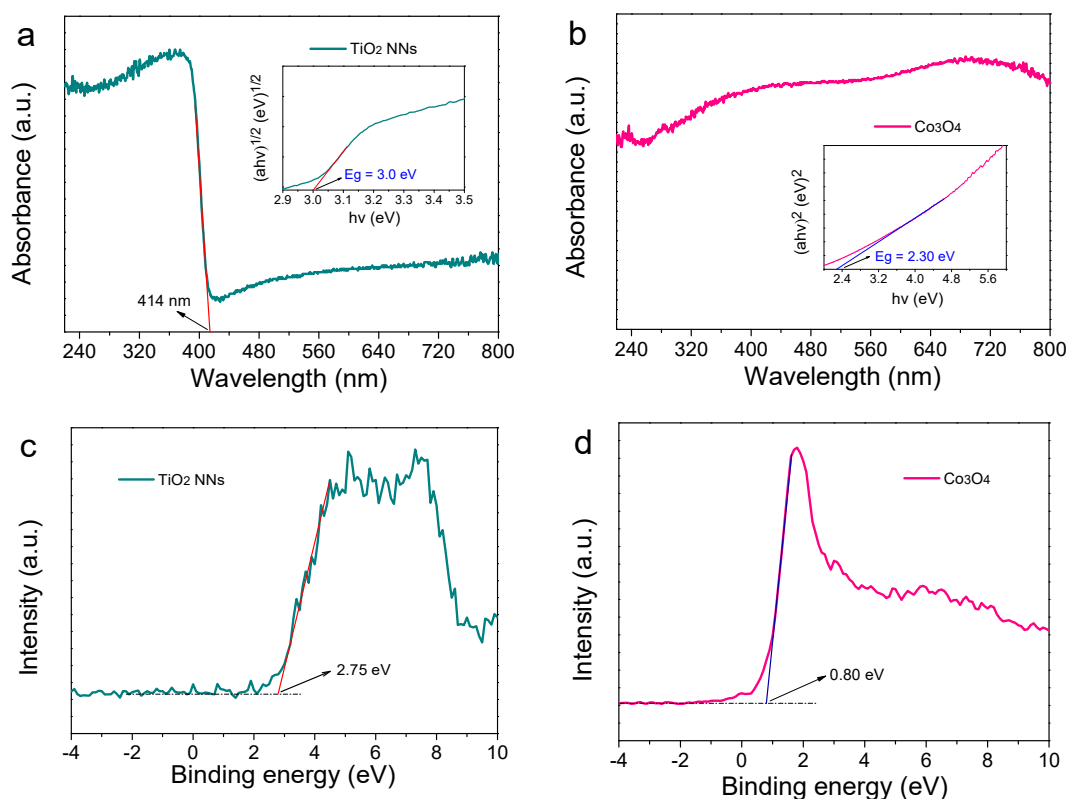


Figure 3. UV-Vis diffuse reflectance spectra of TiO₂ NNs photoanode with the inset of Tauc's plots of $(\alpha h\nu)^{1/2}$ versus $h\nu$ (a), Co₃O₄ photocathode with the inset of Tauc's plots of $(\alpha h\nu)^2$ versus $h\nu$ (b). VB XPS spectra of TiO₂ NNs photoanode (c) and Co₃O₄ photocathode (d).

The transient photocurrent responses and EIS analysis were conducted in Na₂SO₄ solution with or without LED light illumination to examine the separation and transfer ability of photogenerated charge carriers. As shown in Figure 4a, the photocurrent of the dual-photoelectrode PEC system (TiO₂ NNs-Co₃O₄) was 0.060 mA cm⁻², which was about 1.67 times and 20 times higher than those of the TiO₂ NNs-Pt (0.036 mA cm⁻²) and Pt-Co₃O₄ (0.004 mA cm⁻²) PEC system, respectively. In addition, it could be seen from Figure 4b and Table S2 that the radius of the TiO₂ NNs-Co₃O₄ system was smaller than that of the single-photoelectrode (e.g., TiO₂ NNs-Pt, Pt-Co₃O₄) PEC system both in the dark and under LED illumination, indicating that the dual-photoelectrode PEC system had lower charge transfer resistance [26]. Therefore, compared with TiO₂ NNs-Pt and Pt-Co₃O₄, the dual-phot-electrode PEC system had excellent photogenerated charge carriers transfer performance, which was in agreement with recent research [25].

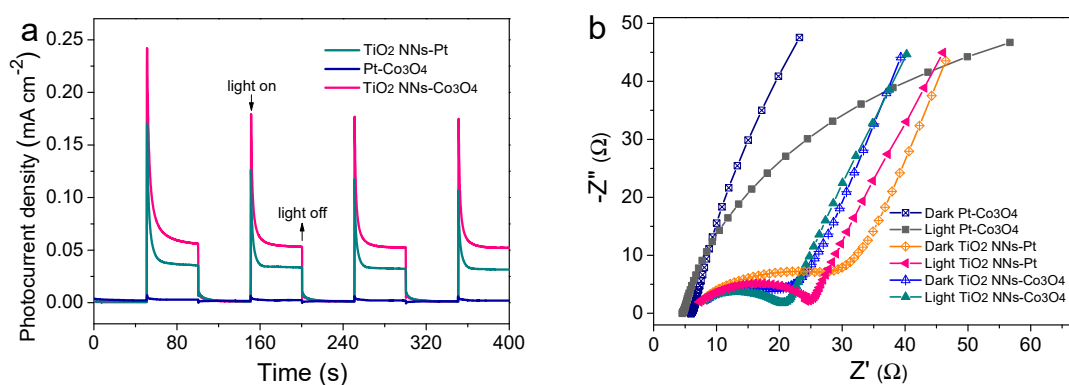


Figure 4. Cont.

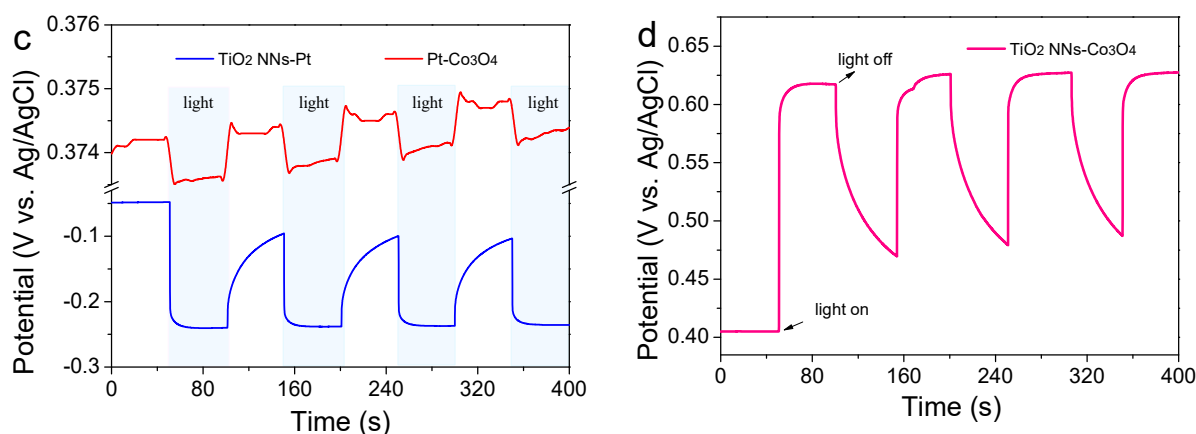


Figure 4. (a) Transient photocurrent responses of TiO₂ NNs-Pt, Pt-Co₃O₄, and TiO₂ NNs-Co₃O₄. (b) EIS Nyquist plots with or without light irradiation. The V_{OC} of (c) TiO₂ NNs-Pt and Pt-Co₃O₄ PEC system in the dark and under LED light illumination, and (d) TiO₂ NNs-Co₃O₄ PEC system.

To further clarify the peculiarity of the novel TiO₂ NNs-Co₃O₄ system, we measured the open-circuit voltage (V_{OC}) of different PEC systems (Figure 4c,d). Notably, the V_{OC} values in the dark of the TiO₂ NNs-Pt and Pt-Co₃O₄ PEC system were measured to be about -0.048 and 0.374 V vs. Ag/AgCl, respectively. Under illumination, the TiO₂ NNs photoanode absorbed LED light to make V_{OC} change to -0.238 V vs. Ag/AgCl, while the V_{OC} of the Co₃O₄ photocathode showed a slight change. As reported in [12], the theoretical V_{OC} of the TiO₂ NNs-Co₃O₄ system was calculated to be about 0.422 V vs. Ag/AgCl in the dark and 0.612 V vs. Ag/AgCl with LED-light irradiation, which was almost consistent with the V_{OC} curve of the dual-photoelectrode PEC system in Figure 4d. Consequently, the internal bias of the TiO₂ NNs-Co₃O₄ system was around 0.19 V, where the TiO₂ NNs photoanode provided a negative bias for the photocathode and the Co₃O₄ photocathode provided a positive bias for the photoanode, in agreement with LSV results (Figure S1) [27]. This phenomenon confirmed that the TiO₂ NNs-Co₃O₄ PEC system would produce larger internal bias than the single-photoelectrode system (TiO₂ NNs-Pt, Pt-Co₃O₄) under light irradiation, which had the potential to enable this dual-photoelectrode PEC system to self-drive and efficiently degrade organic pollutants without external bias [12,24].

2.3. Photoelectrochemical Degradation of SMT in TiO₂ NNs-Co₃O₄ System

2.3.1. Photoelectrochemical Performance

Photoelectrocatalytic activities of the TiO₂ NNs-Pt, Pt-Co₃O₄, and TiO₂ NNs-Co₃O₄ PEC system for SMT degradation were tested under LED lamp irradiation. As seen from Figure 5a, no appreciable photolysis of SMT was observed. In comparison, the degradation efficiency of SMT in the TiO₂ NNs-Pt and Pt-Co₃O₄ PEC system increased to 54.04% and 42.53%, respectively. These enhanced catalytic activities might be due to the production of photogenerated electrons and holes with redox activity by TiO₂ NNs or Co₃O₄ under LED light illumination. Obviously, about 99.62% SMT could be removed within 120 min of the self-driven TiO₂ NNs-Co₃O₄ PEC system, possibly associating with the increased light absorbance ability and elevated separation rate of photogenerated electrons and holes [12]. Moreover, the k of the self-driven TiO₂ NNs-Co₃O₄ PEC system for SMT removal was 0.042 min^{-1} , which was about 6 and 10.5 times as high as that of TiO₂ NNs-Pt (0.007 min^{-1}) and Pt-Co₃O₄ (0.004 min^{-1}), respectively (Figure 5b). Therefore, the dual-photoelectrode PEC system of TiO₂ NNs-Co₃O₄ possessed increased photoelectrocatalytic activity and water purification performance.

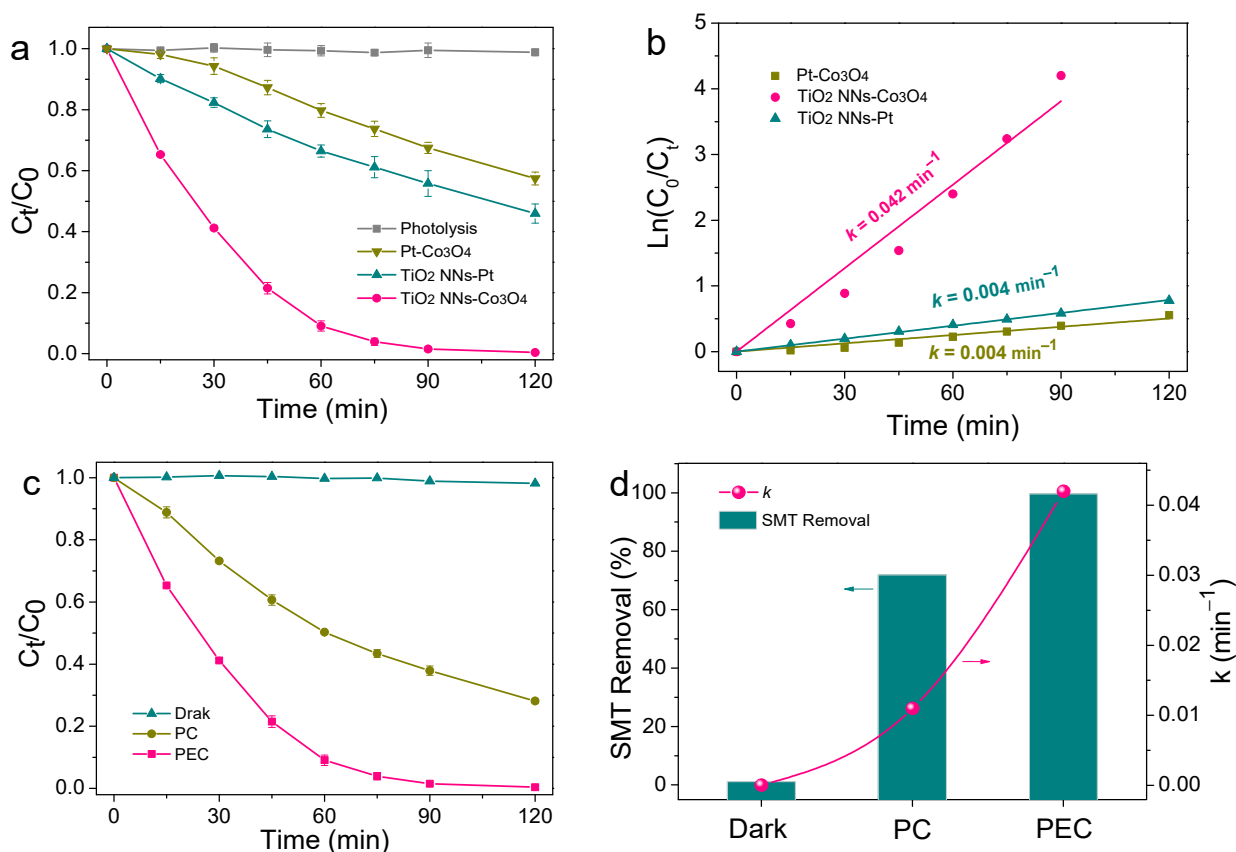


Figure 5. (a) Degradation of SMT by direct photolysis, in Pt-Co₃O₄, TiO₂ NNs-Pt, and TiO₂ NNs-Co₃O₄; (b) the kinetics curves of the above systems. (c,d) Removal of SMT by dark, photocatalysis, and photoelectrochemical process using TiO₂ NNs-Co₃O₄ PEC system.

The degradation efficiency of SMT in the TiO₂ NNs-Co₃O₄ PEC system was also evaluated in the dark (without light), PC (without Cu wire), and self-driven PEC (with light and Cu wire) processes. As shown in Figure 5c,d, the removals of SMT in the TiO₂ NNs-Co₃O₄ system were 1.12, 71.88, and 99.62% after 120 min of reaction, and the corresponding k were about 0, 0.011, and 0.042 min^{-1} in the processes of dark, PC, and self-driven PEC, respectively. The unbiased PEC process showed greatly improved performance in organic pollutant degradation compared to the dark and PC processes. This phenomenon could be attributed to the effectively suppressed recombination of photogenerated charge carriers in the PEC process under the external circuit [28]. Specifically, both the TiO₂ NNs photoanode and Co₃O₄ photocathode could generate electrons and holes under the illumination of an LED lamp. Because the Fermi level of the TiO₂ NNs photoanode was more negative than that of the Co₃O₄ photocathode, the TiO₂ NNs-Co₃O₄ system produced a stable internal photovoltage (0.19 V) [12]. This photovoltage was key to establish a bias-free photoelectrocatalytic degradation system by the TiO₂ NNs photoanode and Co₃O₄ photocathode [29]. In this case, the photovoltage drove the directional transfer of photoinduced charge carriers through the external circuit, thus enhancing the separation rate of photogenerated electron-hole pairs and finally exhibiting higher pollutant degradation activity. The performance comparison of the unbiased dual-photoelectrode PEC system in the literature for pollutant degradation is summarized in Table 1. It was clear that the self-driven TiO₂ NNs-Co₃O₄ system had excellent performance and the energy consumption of the light source (LED lamp) used in this system was significantly lower than that of other unbiased PEC systems (Xe lamp).

Table 1. The performance comparison of recently self-driven PEC system for wastewater treatment.

| System | Electrolyte | Pollutant | Removal | k (min^{-1}) | Light Source | Ref. |
|---|---|--|---------------------|---------------------------|---------------|-----------|
| WO ₃ /W photoanode Cu ₂ O/Cu photocathode | 0.1 M KH ₂ PO ₄ ; | rhodamine B (20 mg/L) | 60% (300 min) | – | 350 W Xe lamp | [12] |
| BiVO ₄ /WO ₃ /W photoanode Pt/BJS photocathode | 0.1 M Na ₂ SO ₄ ; | tetracycline hydrochloride (20 mg/L) | 78% (240 min) | ~0.006 | 350 W Xe lamp | [30] |
| BiVO ₄ /TiO ₂ NT photoanode Cu ₂ O/TiO ₂ NT photocathode | 0.1 M Na ₂ SO ₄ ; | tetracycline hydrochloride (10 mg/L) | ~ 50% (120 min) | ~0.005 | 300 W Xe lamp | [10] |
| BiVO ₄ /TiO ₂ NTs photoanode ZnO/CuO NWs photocathode | 0.1 M Na ₂ SO ₄ ; | methylene blue (20 mg/L) | 83% (80 min) | ~0.029 | 350 W Xe lamp | [31] |
| TiO ₂ /Ti photoanode Cu ₂ O/Cu photocathode | 0.1 M PBS; | methylene blue (10 mg/L) | 87% (480 min) | ~0.005 | 350 W Xe lamp | [32] |
| PANI/TiO ₂ NTs photoanode CuO/Co ₃ O ₄ photocathode | 0.1 M Na ₂ SO ₄ ; | rhodamine B (~5 mg/L) | 68.5% (240 min) | – | – | [24] |
| BiVO ₄ @PDA/TiO ₂ /Ti photoanode Cu ₂ O/Cu cathode photocathode | 0.5 M Na ₂ SO ₄ ; | rhodamine B (10 mg/L) | 97.28% (120 min) | ~0.030 | 500 W Xe lamp | [33] |
| Ag ₃ PO ₄ @g-C ₃ N ₄ photoanode Cu ₂ O photocathode | 0.1 M Na ₂ SO ₄ ; | tetracycline (10 mg/L) | 76% (240 min) | – | 300 W Xe lamp | [34] |
| W/WNR/g-C ₃ N ₄ photoanode ITO/CBFeO photocathode | 0.1 M Na ₂ SO ₄ ; | oxytetracycline (10 mg/L) | 97.6% (90 min) | ~0.042 | 500 W Xe lamp | [35] |
| TiO ₂ NNs photoanode Co ₃ O ₄ photocathode | 0.1 M Na ₂ SO ₄ ; | SMT (10 mg/L) | 99.62% (120 min) | 0.042 | 30 W LED lamp | This work |

2.3.2. Effect of Solution pH

Figure 6a manifested how the initial solution pH affected SMT degradation in the unbiased TiO₂ NNs-Co₃O₄ PEC system. When the pH was 3.0, 5.0, 7.0, 9.0, and 11.0, the degradation efficiency of SMT was 98.92% (0.051 min⁻¹), 98.73% (0.048 min⁻¹), 97.44% (0.041 min⁻¹), 96.77% (0.035 min⁻¹), and 80.89% (0.023 min⁻¹) after 90 min of reaction. It was clear that the decomposition rate of SMT decreased with the increase in initial pH value. This might be due to the fact that pH was closely related to the formation of ROS and the interaction between electrolyte and electrode. Specifically, the •OH and h⁺ worked as the dominating role of SMT degradation, which were obtained by quenching experiments (part 2.4.1). There was a large amount of OH⁻ in the alkaline environment, which could consume h⁺ to generate •OH, and the oxidation ability of •OH was lower than that of h⁺ [15]. In addition, according to the Nernst equation, the oxidation potential of •OH in basic medium was also lower than that in acidic conditions [36]. On the other hand, acidic circumstances had been reported to facilitate charge transfer between the photo-electrode and electrolyte in PEC degradation of organic pollutants [37]. Hence, the novel TiO₂ NNs-Co₃O₄ PEC system had superior operative performance in acidic and slightly alkaline environments.

2.3.3. Effect of Background Species

Inorganic anions and natural organic matter (NOM) were ubiquitous in actual water matrix. Therefore, the effects of 10 mM typical anions (Cl⁻, CO₃²⁻, PO₄³⁻) and 10 mg L⁻¹ of NOM (representing by HA) on the degradation of SMT by the self-driven TiO₂ NNs-Co₃O₄ PEC system were investigated to evaluate the practical application prospects of this system. In the presence of CO₃²⁻, PO₄³⁻, and HA, the degradation rates of SMT were 97.95, 96.28, and 99.52%, and the corresponding k values were 0.36, 0.37, and 0.35 min⁻¹, respectively. This slight inhibition effect might be attributed to the consumption of •OH or h⁺ by CO₃²⁻, PO₄³⁻, or HA, while •OH and h⁺ participated in the degradation of SMT (Figure 6b) [38–40]. Impressively, the presence of Cl⁻ significantly accelerated SMT removal (99.60%, 0.062 min⁻¹), which could be attributed to the formation of active chlorine species (•Cl, •ClO, HClO) in the bias-free TiO₂ NNs-Co₃O₄ PEC system [41–43]. Therefore, bias-free TiO₂ NNs-Co₃O₄ PEC had the potential for saline wastewater treatment.

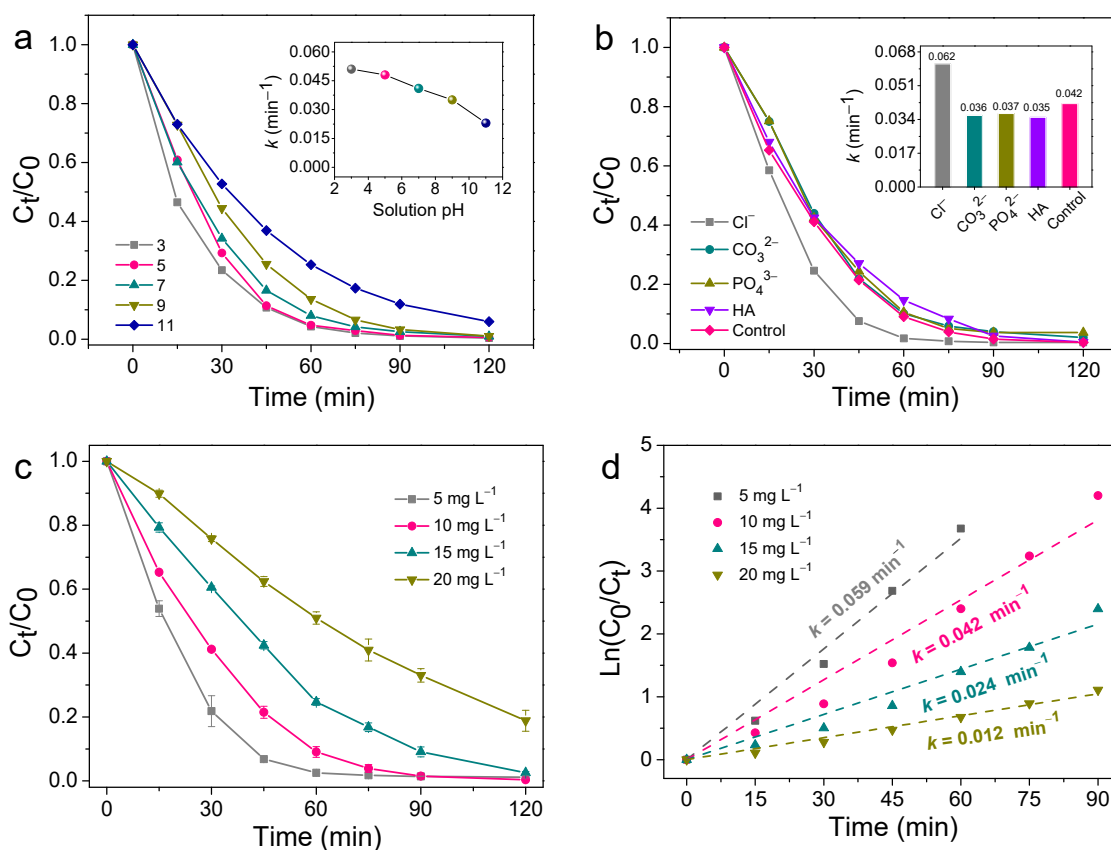


Figure 6. Effects of (a) solution pH and (b) background species, and (c,d) initial SMT concentration on unbiased TiO_2 NNS- Co_3O_4 PEC system for removal of SMT.

2.3.4. Effect of Initial SMT Concentration

The degradation ability of the bias-free TiO_2 NNS- Co_3O_4 PEC system at different SMT initial concentrations is shown in Figure 6c,d. The k for degradation of 5 mg/L of SMT was 0.059 min^{-1} , which was about 1.40, 2.46, and 4.92 times higher than those of 10, 15, and 20 mg/L of SMT, respectively (Figure 6d). Additionally, in the case of 5 mg/L of SMT, about 98% SMT was decomposed within 60 min of irradiation, and the degradation rate still reached more than 97% after 90 (for concentration of 10 mg/L) and 120 min (for concentration of 15 mg/L) of LED light irradiation. When the initial concentration was increased to 20 mg/L , the removal rate was only 81.16% after 120 min of reaction, which could be attributed to the fact that the reactive oxygen species (ROS) generated in the PEC system were exhausted by excessive SMT (Figure 6c) [44]. Although k of SMT removal in this self-driven PEC system decreased with the increase in initial concentration, the degradation efficiency of SMT was high when the illumination time was prolonged.

2.4. Mechanism in TiO_2 NNS- Co_3O_4 System

The quenching experiments were studied to clarify the contribution of the main ROS during SMT degradation in the unbiased TiO_2 NNS- Co_3O_4 PEC system under visible LED light irradiation. Isopropanol (IPA, 100 mM) and ammonium oxalate (AO, 50 mM) were applied as h^+ and $\bullet\text{OH}$ quenchers, respectively, and the results were displayed in Figure 7a. After adding AO to the reaction system, the degradation efficiency of SMT decreased to the lowest (66.96%) within 120 min, indicating that h^+ was the dominant ROS. When IPA was added, the efficiency was reduced to 84.37%, implying that $\bullet\text{OH}$ participated in the degradation process of SMT. Moreover, we further confirmed the role of $\bullet\text{O}_2^-$ in the system by purging N_2 . The decomposition efficiency was slightly suppressed to 90.56%. To sum up, the contribution of different ROS for SMT removal in the unbiased TiO_2 NNS- Co_3O_4

PEC system was in the order: h^+ (0.010 min^{-1}) > $\bullet\text{OH}$ (0.015 min^{-1}) > $\bullet\text{O}_2^-$ (0.025 min^{-1}) (Figure 7b).

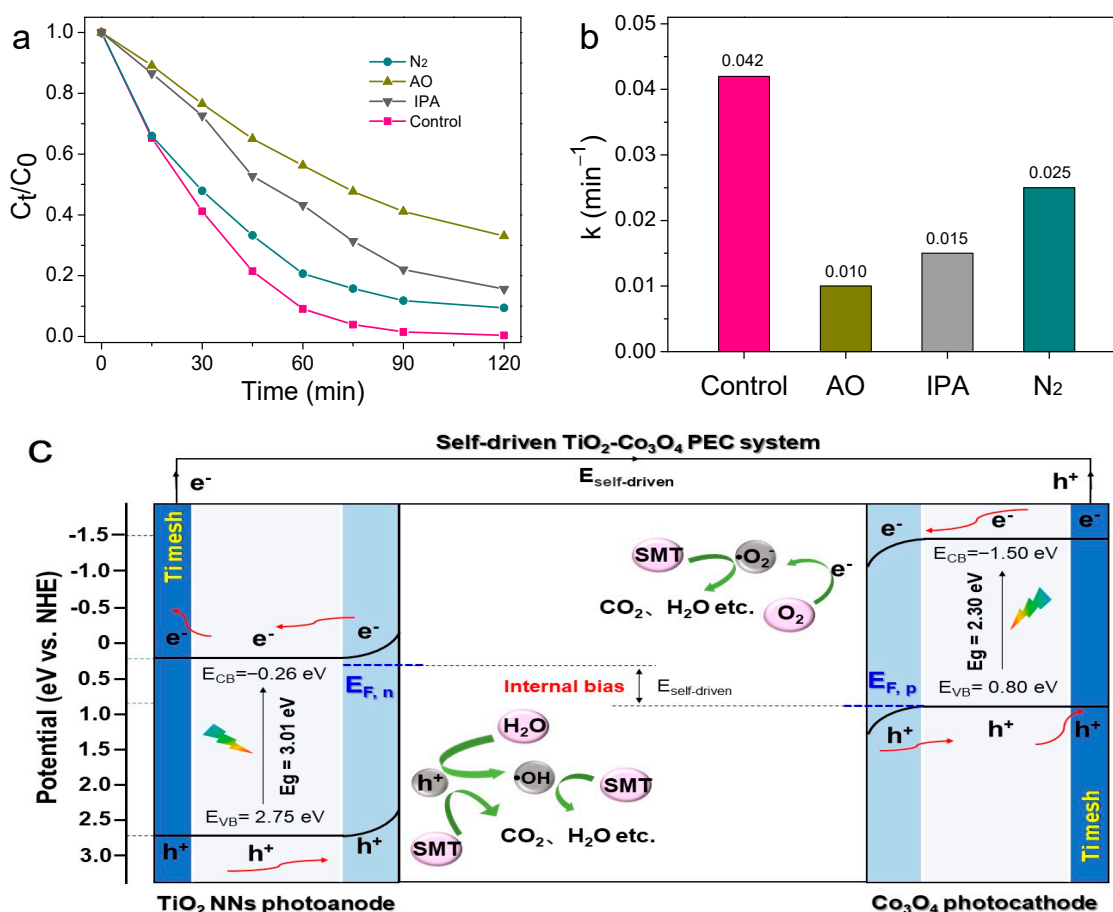


Figure 7. Effects of different quenching scavengers on SMT degradation efficiency (a) and reaction rate constant (b). Possible mechanism of SMT degradation of unbiased TiO_2 NNs- Co_3O_4 PEC system under visible LED light irradiation (c).

Given these results, the operating mechanism of the unbiased TiO_2 NNs- Co_3O_4 PEC system for SMT degradation was inferred in-depth. As observed in Figure 7c, under the LED light irradiation, the dual-photoelectrode PEC system produced internal bias (0.19 V) due to the difference in the Fermi level of the TiO_2 NNs photoanode and Co_3O_4 photocathode [30]. Then, the photoinduced electrons of the TiO_2 NNs photoanode were swiftly transferred to the Co_3O_4 photocathode driven by internal bias, which improved the separation rate of electron–hole pairs [45]. As a result, there would be more photoinduced holes in the photoanode and photogenerated electrons in the photocathode to participate in the oxidation–reduction reaction to generate ROS ($\bullet\text{OH}$, $\bullet\text{O}_2^-$), leading to the efficient degradation of SMT.

2.5. Practicability of TiO_2 NNs- Co_3O_4 PEC System

The practicability of the unbiased TiO_2 NNs- Co_3O_4 PEC system was evaluated by the cycling experiment. As presented in Figure 8a, the degradation efficiency of SMT in the first, second, third, fourth, and fifth cycle experiments was 99.62%, 99.38%, 99.52%, 99.33%, and 99.40%, respectively. It was clear that the degradation capacity of SMT was almost unchanged after five degradation cycles, indicating that the bias-free TiO_2 NNs- Co_3O_4 PEC system had superior stability. Furthermore, the catalytic performance of this unbiased dual-photoelectrode PEC system was detected in pharmaceutical wastewater

and mariculture wastewater. The quality parameters of actual pharmaceutical wastewater (PW) and mariculture wastewater (MW) are listed in Table S1. As can be seen from Figure 8b, the k value of SMT degradation in pharmaceutical wastewater and mariculture wastewater was 0.035 min^{-1} and 0.052 min^{-1} , respectively. The inhibitory action of pharmaceutical wastewater might be due to its complex composition, and the promoting effect of mariculture wastewater could be attributed to the presence of high concentrations of Cl^- . This phenomenon was consistent with the results of the influence of background species. The remarkable catalytic performance for SMT degradation in pharmaceutical wastewater (99.70%, 120 min) and mariculture wastewater (98.98%, 75 min) indicated that self-driven TiO_2 NNs- Co_3O_4 was a promising PEC system for water purification.

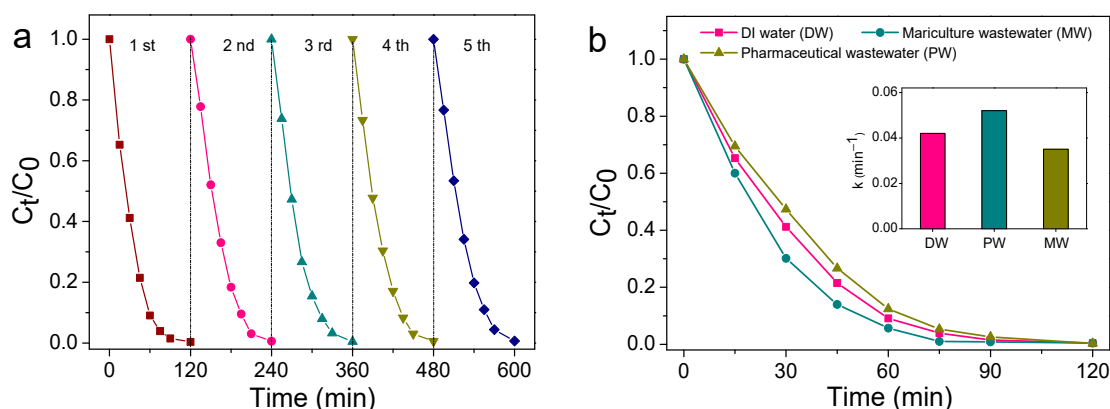


Figure 8. Five consecutive cycling tests using TiO_2 NNs- Co_3O_4 PEC system (a). PEC degradation of SMT in actual pharmaceutical wastewater and mariculture wastewater of TiO_2 NNs- Co_3O_4 system (b).

3. Experimental Section

3.1. Photoelectrodes Preparation

The TiO_2 NNs were grown on Ti mesh through a hydrothermal method reported previously [17]. Ti mesh ($2.8 \text{ cm} \times 4 \text{ cm} \times 0.1 \text{ mm}$) was pretreated with acetone, ethanol, and deionized water before use. Briefly, 0.3 mL of titanium isopropoxide was dissolved in acetylacetone to form a yellow solution. Then, the above solution was slowly added to Na_2EDTA solution and stirred for 30 min. The solution was then transferred into a Teflon-lined stainless-steel autoclave, which was heated at $200 \text{ }^\circ\text{C}$ for 12 h. The sample was annealed in a Muffle furnace at $500 \text{ }^\circ\text{C}$ (ramping rate: $2 \text{ }^\circ\text{C min}^{-1}$) for 1 h to obtain the TiO_2 NNs electrode.

The Co_3O_4 electrode was synthesized by using a NH_4F -assisted hydrothermal method recently reported [46]. Typically, 2.9 mmol $\text{Co}(\text{NO}_3)_2 \cdot 6\text{H}_2\text{O}$, 5.7 mmol NH_4F , and 14.3 mmol $\text{CO}(\text{NH}_2)_2$ were dissolved in deionized water to form a homogeneous solution. Then, this solution along with pretreated Ti mesh was transferred into a 50 mL Teflon-lined autoclave, which was heated at $120 \text{ }^\circ\text{C}$ for 5 h. Subsequently, the obtained sample was calcined in air atmosphere at $350 \text{ }^\circ\text{C}$ for 2 h.

3.2. Characterizations

SEM images and structures of the prepared electrodes were investigated by field-emission scanning electron microscopy (FESEM, LEO-1530VP), and X-ray diffraction (XRD, Philips-12045 B/3 diffractometer with $\text{Cu-K}\alpha$ irradiation). The X-ray photoelectron spectra (XPS) were determined on a Thermo Scientific ESCALAB 250Xi with a monochromatic $\text{Al-K}\alpha$ source. The UV-vis diffuse reflectance spectra (UV-vis DRS) were collected on a Shimadzu 2600 UV spectrophotometer by using BaSO_4 as a reference. The cobalt leaching concentration after photoelectrocatalytic reaction was analyzed by ICP-MS (PerkinElmer ELAN DRC-e, Waltham, MA, USA). The ROS were detected by electron paramagnetic

resonance (EPR, Bruker EMX Nano, Heidelberg, Germany) by employing 5,5-dimethyl-1-pyrroline N-oxide (DMPO) as a spin-trapping agent.

3.3. Photoelectrochemical Measurement

The photoelectrochemical measurement was analyzed using the standard three-electrode system on a CHI760E electrochemical station. All tests were carried out in 0.1 M Na₂SO₄ electrolyte by using Ag/AgCl as a reference electrode, and Pt foil and the as-prepared photoelectrode as the counter electrode and working electrode, respectively. The light source was two 30 W LED lamps. Electrochemical impedance spectroscopy (EIS) was measured at an open-circuit voltage from 100 kHz to 0.01 Hz. The transient photocurrent responses were collected without external bias under LED light illumination and in the dark. Linear sweep voltammetry (LSV) curves were recorded with the scan rate of 10 mV s⁻¹.

3.4. Construction and Evaluation of Established PEC Systems

For simplicity, we named the TiO₂ NNs photoanode-coupled Pt cathode, Pt anode-coupled Co₃O₄ photocathode, and TiO₂ NNs photoanode-coupled Co₃O₄ photocathode as TiO₂ NNs-Pt, Pt-Co₃O₄, and TiO₂ NNs-Co₃O₄, respectively. Then, taking SMT as the model pollutant, the degradation experiments were carried out in a single-chamber electrolysis cell with a two-electrode system to evaluate the performance of the above-mentioned PEC systems. The 70 mL reaction solution contained 0.1 M Na₂SO₄ and 10 mg/L of SMT. The established PEC systems were connected via Cu wire without applied voltage, and the LED light was turned on to start the photoelectrocatalytic reaction.

3.5. Analytical Methods

The concentration of SMT was determined by high-performance liquid chromatography (HPLC, Ultimate 3000 ThermoFisher, Acclaim™ 120 C18 column at 30 °C, a 35:65 v/v acetonitrile/water solution as the mobile phase, flow rate of 0.5 mL/min, and detection wavelength of 270 nm). The degradation kinetics of SMT was fitted by the first-order reaction using Equation (3).

$$-\ln \left(\frac{C_t}{C_0} \right) = kt \quad (3)$$

where C_t (mg/L) is the SMT concentration at a certain time t (min), C_0 (mg/L) is the initial SMT concentrations, and k is the pseudo-first-order rate constant of SMT (min⁻¹).

4. Conclusions

In short, an unbiased dual-photoelectrode (TiO₂ NNs-Co₃O₄) PEC system encompassing a TiO₂ NNs photoanode and Co₃O₄ photocathode was established for the first time, which could efficiently degrade SMT (99.62%, 0.042 min⁻¹) under LED light irradiation. The photoelectrocatalytic activity of the self-driven TiO₂ NNs-Co₃O₄ PEC system for SMT degradation was around 6 and 10.5 times as high as those of the TiO₂ NNs-Pt (0.007 min⁻¹) and Pt-Co₃O₄ (0.004 min⁻¹) system, respectively. The improved catalytic performance could be attributed to the internal photovoltage (0.19 V) generated by the potential difference of Fermi level between the photoelectrode. In addition, the slight influence of solution pH, typical inorganic anions, and NOM on SMT degradation efficiency (≥94.03%) suggested that the bias-free TiO₂ NNs-Co₃O₄ PEC system had excellent catalytic performance under environment-related conditions. In addition, quenching experiments indicated that h⁺, •OH, and •O₂⁻ were predominant ROS during the decomposition process of SMT in this dual-photoelectrode PEC system. Moreover, the outstanding performance in reusability (99.40% of the fifth cycles), pharmaceutical wastewater (99.56%), and mariculture wastewater (99.70%) further revealed its potential for practical environmental remediation. This work provides novel inspirations for designing an efficient, sustainable, and strong-stable PEC system to purify wastewater.

Supplementary Materials: The following supporting information can be downloaded at: <https://www.mdpi.com/article/10.3390/catal13020327/s1>, Figure S1: Linear sweep voltammetry (LSV) curves of the as-prepared TiO₂ NNs photoanode (a) and Co₃O₄ photocathode (b); Table S1: The quality parameters of the actual environmental matrices; Table S2: Equivalent circuits fitting of EIS data for TiO₂ NNs-Co₃O₄, TiO₂ NNs-Pt, and Pt-Co₃O₄ system with or without LED lamp illumination.

Author Contributions: Z.H.: Conceptualization, Methodology, Formal analysis, Investigation, Data curation, Writing—original draft, Writing—review & editing. R.L.: Conceptualization, Methodology, Formal analysis, Investigation, Data curation. X.S. and H.W.: Investigation, Resources, Data curation. J.S. and J.L.: Data curation. M.Z.: Conceptualization, Supervision, Funding acquisition, Resources, Writing—review & editing. O.A.A.: Writing—review & editing. All authors have read and agreed to the published version of the manuscript.

Funding: This work was financially supported by the National Key R&D Program International Cooperation Project (2021YFE0106500); Key Project of Natural Science Foundation of Tianjin (No. 21JCZDJC00320); Fundamental Research Funds for the Central Universities, Nankai University, and National Research Foundation IRG—China/South Africa Research Cooperation Program (Grant Number 132793).

Data Availability Statement: Not applicable.

Conflicts of Interest: The authors declare no conflict of interest or other interest that might be perceived to influence the results and/or discussion reported in this paper.

References

1. Xu, G.; Zhang, B.; Wang, X.; Li, N.; Liu, L.; Lin, J.-M.; Zhao, R.-S. Nitrogen-doped flower-like porous carbon nanostructures for fast removal of sulfamethazine from water. *Environ. Pollut.* **2019**, *255*, 113229. [[CrossRef](#)] [[PubMed](#)]
2. Pan, Y.; Zhang, Y.; Zhou, M.; Cai, J.; Tian, Y. Enhanced removal of emerging contaminants using persulfate activated by UV and pre-magnetized Fe⁰. *Chem. Eng. J.* **2019**, *361*, 908–918. [[CrossRef](#)]
3. Xiong, J.-Q.; Kurade, M.B.; Jeon, B.-H. Can Microalgae Remove Pharmaceutical Contaminants from Water? *Trends Biotechnol.* **2018**, *36*, 30–44. [[CrossRef](#)] [[PubMed](#)]
4. Belhaj, D.; Baccar, R.; Jaabiri, I.; Bouzid, J.; Kallel, M.; Ayadi, H.; Zhou, J.L. Fate of selected estrogenic hormones in an urban sewage treatment plant in Tunisia (North Africa). *Sci. Total Environ.* **2015**, *505*, 154–160. [[CrossRef](#)] [[PubMed](#)]
5. Zhang, T.; Yang, Y.; Li, X.; Yu, H.; Wang, N.; Li, H.; Du, P.; Jiang, Y.; Fan, X.; Zhou, Z. Degradation of sulfamethazine by persulfate activated with nanosized zero-valent copper in combination with ultrasonic irradiation. *Sep. Purif. Technol.* **2020**, *239*, 116537. [[CrossRef](#)]
6. Grandclément, C.; Seyssiecq, I.; Piram, A.; Wong-Wah-Chung, P.; Vanot, G.; Tiliacos, N.; Roche, N.; Doumenq, P. From the conventional biological wastewater treatment to hybrid processes, the evaluation of organic micropollutant removal: A review. *Water Res.* **2017**, *111*, 297–317. [[CrossRef](#)]
7. Pan, Y.; Bu, Z.; Sang, C.; Guo, H.; Zhou, M.; Zhang, Y.; Tian, Y.; Cai, J.; Wang, W. EDTA enhanced pre-magnetized Fe⁰/H₂O₂ process for removing sulfamethazine at neutral pH. *Sep. Purif. Technol.* **2020**, *250*, 117281. [[CrossRef](#)]
8. Zhang, X.; Nengzi, L.-c.; Li, B.; Liu, L.; Cheng, X. Design and construction of a highly efficient photoelectrocatalytic system based on dual-Pd/TNAs photoelectrodes for elimination of triclosan. *Sep. Purif. Technol.* **2020**, *235*, 116232. [[CrossRef](#)]
9. Wu, S.; Hu, Y.H. A comprehensive review on catalysts for electrocatalytic and photoelectrocatalytic degradation of antibiotics. *Chem. Eng. J.* **2021**, *409*, 127739. [[CrossRef](#)]
10. Lu, Y.; Chu, Y.; Zheng, W.; Huo, M.; Huo, H.; Qu, J.; Yu, H.; Zhao, Y. Significant tetracycline hydrochloride degradation and electricity generation in a visible-light-driven dual photoelectrode photocatalytic fuel cell using BiVO₄/TiO₂ NT photoanode and Cu₂O/TiO₂ NT photocathode. *Electrochim. Acta* **2019**, *320*, 134617. [[CrossRef](#)]
11. Kim, J.H.; Jang, J.W.; Jo, Y.H.; Abdi, F.F.; Lee, Y.H.; van de Krol, R.; Lee, J.S. Hetero-type dual photoanodes for unbiased solar water splitting with extended light harvesting. *Nat. Commun.* **2016**, *7*, 13380. [[CrossRef](#)] [[PubMed](#)]
12. Chen, Q.; Li, J.; Li, X.; Huang, K.; Zhou, B.; Cai, W.; Shangguan, W. Visible-light responsive photocatalytic fuel cell based on WO₃/W photoanode and Cu₂O/Cu photocathode for simultaneous wastewater treatment and electricity generation. *Environ. Sci. Technol.* **2012**, *46*, 11451–11458. [[CrossRef](#)]
13. Luo, T.; Bai, J.; Li, J.; Zeng, Q.; Ji, Y.; Qiao, L.; Li, X.; Zhou, B. Self-Driven photoelectrochemical splitting of H₂S for S and H₂ recovery and simultaneous electricity generation. *Environ. Sci. Technol.* **2017**, *51*, 12965–12971. [[CrossRef](#)] [[PubMed](#)]
14. Suarez-Chamba, M.; Tuba-Guamán, D.; Quishpe, M.; Vizuete, K.; Debut, A.; Herrera-Robledo, M. Photocatalytic degradation of bisphenol A on BiOI nanostructured films under visible LED light irradiation. *J. Photochem. Photobiol. A Chem.* **2022**, *431*, 114021. [[CrossRef](#)]
15. Hu, Z.; Xie, X.; Li, S.; Song, M.; Liang, G.; Zhao, J.; Wang, Z. Rational construct CQDs/BiOCCOOH/uCN photocatalyst with excellent photocatalytic performance for degradation of sulfathiazole. *Chem. Eng. J.* **2021**, *404*, 126541. [[CrossRef](#)]

16. Hou, Y.; Zuo, F.; Dagg, A.; Feng, P. A three-dimensional branched cobalt-doped alpha-Fe₂O₃ nanorod/MgFe₂O₄ heterojunction array as a flexible photoanode for efficient photoelectrochemical water oxidation. *Angew. Chem. Int. Ed.* **2013**, *52*, 1248–1252. [[CrossRef](#)]
17. Song, R.; Chi, H.; Ma, Q.; Li, D.; Wang, X.; Gao, W.; Wang, H.; Wang, X.; Li, Z.; Li, C. Highly efficient degradation of persistent pollutants with 3D nanocone TiO₂-Based photoelectrocatalysis. *J. Am. Chem. Soc.* **2021**, *143*, 13664–13674. [[CrossRef](#)]
18. Wang, Y.; Zhou, T.; Jiang, K.; Da, P.; Peng, Z.; Tang, J.; Kong, B.; Cai, W.-B.; Yang, Z.; Zheng, G. Reduced mesoporous Co₃O₄ nanowires as efficient water oxidation electrocatalysts and supercapacitor electrodes. *Adv. Energy Mater.* **2014**, *4*, 1400696. [[CrossRef](#)]
19. Zhong, D.; Cai, B.; Wang, X.; Yang, Z.; Xing, Y.; Miao, S.; Zhang, W.-H.; Li, C. Synthesis of oriented TiO₂ nanocones with fast charge transfer for perovskite solar cells. *Nano Energy* **2015**, *11*, 409–418. [[CrossRef](#)]
20. Wang, Z.; Liu, H.; Ge, R.; Ren, X.; Ren, J.; Yang, D.; Zhang, L.; Sun, X. Phosphorus-Doped Co₃O₄ Nanowire Array: A highly efficient bifunctional electrocatalyst for overall water splitting. *ACS Catal.* **2018**, *8*, 2236–2241. [[CrossRef](#)]
21. Zhou, T.; Chen, S.; Li, L.; Wang, J.; Zhang, Y.; Li, J.; Bai, J.; Xia, L.; Xu, Q.; Rahim, M.; et al. Carbon quantum dots modified anatase/rutile TiO₂ photoanode with dramatically enhanced photoelectrochemical performance. *Appl. Catal. B-Environ.* **2020**, *269*, 118776. [[CrossRef](#)]
22. Zhang, X.; Xiao, J.; Zhang, X.; Meng, Y.; Xiao, D. Three-Dimensional Co₃O₄ Nanowires@Amorphous Ni(OH)₂ Ultrathin Nanosheets Hierarchical Structure for Electrochemical Energy Storage. *Electrochim. Acta* **2016**, *191*, 758–766. [[CrossRef](#)]
23. Zheng, Z.; Lo, I.M.C. Fabrication of MoS₂@BL-BiVO₄ photoanode with promoted charge separation for photoelectrochemical sewage treatment to simultaneously degrade PPCPs, disinfect E. coli, and produce H₂: Performance, mechanisms, and influence factors. *Appl. Catal. B-Environ.* **2021**, *299*, 120636. [[CrossRef](#)]
24. Pan, H.; Liao, W.; Sun, N.; Murugananthan, M.; Zhang, Y. Highly efficient and visible light responsive heterojunction composites as dual photoelectrodes for photocatalytic fuel cell. *Catalysts* **2018**, *8*, 30. [[CrossRef](#)]
25. Zhang, J.; Zhang, G.; Lan, H.; Qu, J.; Liu, H. Synergetic hydroxyl radical oxidation with atomic hydrogen reduction lowers the organochlorine conversion barrier and potentiates effective contaminant mineralization. *Environ. Sci. Technol.* **2021**, *55*, 3296–3304. [[CrossRef](#)]
26. Chatzitakis, A.; Papaderakis, A.; Karanasios, N.; Georgieva, J.; Pavlidou, E.; Litsardakis, G.; Poullos, I.; Sotiropoulos, S. Comparison of the photoelectrochemical performance of particulate and nanotube TiO₂ photoanodes. *Catal. Today* **2017**, *280*, 14–20. [[CrossRef](#)]
27. Zheng, J.; Zhou, H.; Zou, Y.; Wang, R.; Lyu, Y.; Jiang, S.P.; Wang, S. Efficiency and stability of narrow-gap semiconductor-based photoelectrodes. *Energy Environ. Sci.* **2019**, *12*, 2345–2374. [[CrossRef](#)]
28. Pan, D.; Xiao, S.; Chen, X.; Li, R.; Cao, Y.; Zhang, D.; Pu, S.; Li, Z.; Li, G.; Li, H. Efficient photocatalytic fuel cell via simultaneous visible-photoelectrocatalytic degradation and electricity generation on a porous coral-like WO₃/W photoelectrode. *Environ. Sci. Technol.* **2019**, *53*, 3697–3706. [[CrossRef](#)]
29. Liang, X.; Wang, P.; Tong, F.; Liu, X.; Wang, C.; Wang, M.; Zhang, Q.; Wang, Z.; Liu, Y.; Zheng, Z.; et al. Bias-free solar water splitting by Tetragonal Zircon BiVO₄ nanocrystal photocathode and Monoclinic Scheelite BiVO₄ nanoporous photoanode. *Adv. Funct. Mater.* **2020**, *31*, 2008656. [[CrossRef](#)]
30. Xia, L.; Bai, J.; Li, J.; Zeng, Q.; Li, X.; Zhou, B. A highly efficient BiVO₄/WO₃/W heterojunction photoanode for visible-light responsive dual photoelectrode photocatalytic fuel cell. *Appl. Catal. B-Environ.* **2016**, *183*, 224–230. [[CrossRef](#)]
31. Bai, J.; Wang, R.; Li, Y.; Tang, Y.; Zeng, Q.; Xia, L.; Li, X.; Li, J.; Li, C.; Zhou, B. A solar light driven dual photoelectrode photocatalytic fuel cell (PFC) for simultaneous wastewater treatment and electricity generation. *J. Hazard. Mater.* **2016**, *311*, 51–62. [[CrossRef](#)]
32. Li, J.; Li, J.; Chen, Q.; Bai, J.; Zhou, B. Converting hazardous organics into clean energy using a solar responsive dual photoelectrode photocatalytic fuel cell. *J. Hazard. Mater.* **2013**, *262*, 304–310. [[CrossRef](#)] [[PubMed](#)]
33. Liu, Y.; Xu, Y.; Zhong, D.; Yao, H.; Zeng, Y.; Zhong, N.; Luo, H. BiVO₄@PDA/TiO₂/Ti photoanode with polydopamine as electron transfer mediator for efficient visible-light driven photocatalytic fuel cell. *Colloids Surf. A Physicochem. Eng. Asp.* **2021**, *612*, 125941. [[CrossRef](#)]
34. Yu, H.; Xue, Y.; Lu, Y.; Wang, X.; Zhu, S.; Qin, W.; Huo, M. Novel application of a Z-scheme photocatalyst of Ag₃PO₄@g-C₃N₄ for photocatalytic fuel cells. *J. Environ. Manag.* **2020**, *254*, 109738. [[CrossRef](#)]
35. Huang, M.; Zhou, C.; Wen, R.; Tian, J.; Huang, W.; Wei, H.; Lu, J. Membraneless Photocatalytic Fuel Cell with Double Photoelectrodes for Simultaneous Electricity Generation and Pollutant Degradation. *J. Electrochem. Soc.* **2022**, *169*, 026502. [[CrossRef](#)]
36. Kumar, A.; Khan, M.; He, J.; Lo, I.M.C. Recent developments and challenges in practical application of visible-light-driven TiO₂-based heterojunctions for PPCP degradation: A critical review. *Water Res.* **2020**, *170*, 115356. [[CrossRef](#)]
37. Mazierski, P.; Borzyszkowska, A.F.; Wilczewska, P.; Bialk-Bielinska, A.; Zaleska-Medynska, A.; Siedlecka, E.M.; Pieczynska, A. Removal of 5-fluorouracil by solar-driven photoelectrocatalytic oxidation using Ti/TiO₂(NT) photoelectrodes. *Water Res.* **2019**, *157*, 610–620. [[CrossRef](#)] [[PubMed](#)]
38. Jia, M.; Yang, Z.; Xu, H.; Song, P.; Xiong, W.; Cao, J.; Zhang, Y.; Xiang, Y.; Hu, J.; Zhou, C.; et al. Integrating N and F co-doped TiO₂ nanotubes with ZIF-8 as photoelectrode for enhanced photo-electrocatalytic degradation of sulfamethazine. *Chem. Eng. J.* **2020**, *388*, 124388. [[CrossRef](#)]

39. Wu, H.; Hu, Z.; Liang, R.; Nkwachukwu, O.V.; Arotiba, O.A.; Zhou, M. Novel Bi₂Sn₂O₇ quantum dots/TiO₂ nanotube arrays S-scheme heterojunction for enhanced photoelectrocatalytic degradation of sulfamethazine. *Appl. Catal. B-Environ.* **2023**, *321*, 122053. [[CrossRef](#)]
40. Wang, J.; Wang, S. Effect of inorganic anions on the performance of advanced oxidation processes for degradation of organic contaminants. *Chem. Eng. J.* **2021**, *411*, 128392. [[CrossRef](#)]
41. Wu, J.; Tao, Y.; Zhang, C.; Zhu, Q.; Zhang, D.; Li, G. Activation of chloride by oxygen vacancies-enriched TiO₂ photoanode for efficient photoelectrochemical treatment of persistent organic pollutants and simultaneous H₂ generation. *J. Hazard. Mater.* **2023**, *443*, 130363. [[CrossRef](#)]
42. Koo, M.S.; Chen, X.; Cho, K.; An, T.; Choi, W. In situ photoelectrochemical chloride activation using a WO₃ electrode for oxidative treatment with simultaneous H₂ evolution under visible light. *Environ. Sci. Technol.* **2019**, *53*, 9926–9936. [[CrossRef](#)] [[PubMed](#)]
43. Zheng, Z.; Man, J.H.K.; Lo, I.M.C. Integrating reactive chlorine species generation with H₂ evolution in a multifunctional photoelectrochemical system for low operational carbon emissions saline sewage treatment. *Environ. Sci. Technol.* **2022**, *56*, 16156–16166. [[CrossRef](#)] [[PubMed](#)]
44. Ma, Q.; Song, R.; Ren, F.; Wang, H.; Gao, W.; Li, Z.; Li, C. Photoelectrocatalytic degradation of refractory pollutants over WO₃/W network photoelectrode with heterophase junction for enhancing mass transportation and charge separation. *Appl. Catal. B-Environ.* **2022**, *309*, 121292. [[CrossRef](#)]
45. Wu, Z.; Zhao, G.; Zhang, Y.; Liu, J.; Zhang, Y.-n.; Shi, H. A solar-driven photocatalytic fuel cell with dual photoelectrode for simultaneous wastewater treatment and hydrogen production. *J. Mater. Chem. A* **2015**, *3*, 3416–3424. [[CrossRef](#)]
46. Gao, J.; Jiang, B.; Ni, C.; Qi, Y.; Bi, X. Enhanced reduction of nitrate by noble metal-free electrocatalysis on P doped three-dimensional Co₃O₄ cathode: Mechanism exploration from both experimental and DFT studies. *Chem. Eng. J.* **2020**, *382*, 123034. [[CrossRef](#)]

Disclaimer/Publisher's Note: The statements, opinions and data contained in all publications are solely those of the individual author(s) and contributor(s) and not of MDPI and/or the editor(s). MDPI and/or the editor(s) disclaim responsibility for any injury to people or property resulting from any ideas, methods, instructions or products referred to in the content.